Hyperfine splittings of heavy quarkonium hybrids

Joan Soto and Sandra Tomàs Valls

Departament de Física Quàntica i Astrofísica and Institut de Ciències del Cosmos, Universitat de Barcelona, Martí i Franquès 1, 08028 Barcelona, Catalonia, Spain

(Received 12 February 2023; accepted 27 June 2023; published 20 July 2023)

In the framework of the Born-Oppenheimer effective field theory, the hyperfine structure of heavy quarkonium hybrids at leading order in the $1/m_Q$ expansion is determined by two potentials. We estimate those potentials by interpolating between the known short-distance behavior and the long-distance behavior calculated in the QCD effective string theory. The long-distance behavior depends, at leading order, on two parameters which can be obtained from the long-distance behavior of the heavy quarkonium potentials (up to sign ambiguities). The short-distance behavior depends, at leading order, on two extra parameters, which are obtained from a lattice calculation of the lower-lying charmonium hybrid multiplets. This allows us to predict the hyperfine splitting both of bottomonium hybrids and of higher multiplets of charmonium hybrids. We carry out a careful error analysis and compare with other approaches.

DOI: 10.1103/PhysRevD.108.014025

I. INTRODUCTION

Exotic hadrons (those beyond mesons and baryons) have been a matter of research since the early days of QCD [1]. Among them, the so-called hybrids are the closest to standard hadrons, as the only difference resides in their nontrivial gluon content. Hence, their flavor structure is the same as in standard hadrons, but their J^{PC} quantum numbers may differ, since, in general, the nontrivial gluon content contributes to them. Nevertheless, the experimental confirmation of hybrids is an arduous task. On the one hand, hadrons with exotic quantum numbers, which could be associated to hybrid states, are difficult to produce with current beams. On the other hand, for light hadrons, hybrids with standard quantum numbers may mix with standard hadrons in an arbitrary way. However, when heavy quarks are involved, the mixing is suppressed by inverse powers of the heavy quark mass, and, hence, the identification of hybrids with standard quantum numbers should become simpler, provided we have reliable theoretical predictions for the hybrid spectrum.

An economical approach to calculating the hybrid spectrum is the so-called Born-Oppenheimer effective field theory (BOEFT) [2–7]. It exploits the fact that heavy quarks move slowly in heavy hadrons. The effect of the nontrivial gluon (or/and light quark) content is encoded in a series of potentials organized in an $1/m_Q$ expansion, m_Q being the heavy quark mass. The leading potential $[\mathcal{O}(1/m_Q^0)]$ is heavy quark spin and heavy quark mass independent. It has been used to calculate the spin average spectrum [2–4,8], decays to heavy quarkonium [4,9–11], and transitions between heavy quarkonium states [12]. The mixing of heavy quarkonium hybrids with heavy quarkonium starts at the order of $1/m_Q$ [4]. Spin effects also start at the order of $1/m_Q$ [4,5], and, hence, they are more important than in heavy quarkonium, in which they start at the order of $1/m_Q^2$. In that respect, it is important to have spin effects under good control in order to properly identify possible experimental candidates (see Refs. [13,14] for recent reviews).

We calculate here the hyperfine splittings (HFS) for the lower-lying charmonium and bottomonium hybrids at leading order (LO) $[\mathcal{O}(1/m_Q)]$ in the BOEFT. At this order, the HFS depend on two unknown potentials [5,6]. At short distances, the form of these potentials is constrained by the multipole expansion and has been given in Refs. [6,15], where one can also find the form of the relevant next-to-leading-order (NLO) potentials $[\mathcal{O}(1/m_Q^2)]$. The HFS were calculated in that reference using the short-distance form of the potentials only. At long distances, the form of the potentials can be estimated using the QCD effective string theory (EST) [16,17]. This has been carried out for heavy quarkonium [18,19] and for the hybrid-quarkonium mixing terms [4]. We provide the results here for the spin-dependent terms of the lower-lying static hybrid states (Σ_u and Π_u), which turn out to be parameter-free (up to signs). We emphasize that the typical distance between heavy quarks in heavy quarkonium hybrids states is of $\mathcal{O}(1/\Lambda_{\rm QCD})$, and, hence, an interpolation between the short- and long-distance forms of the spin-dependent potentials should provide more

reliable estimates than sticking to the short-distance form only. We propose a simple interpolation and calculate the HFS with it. We use the charmonium spectrum in Ref. [20] to fix the unknown parameters in the short-distance form of the potential and to estimate the interpolation dependence. Then we can predict the HFS of higher multiplets and the HFS of bottomonium hybrids.

We distribute the paper as follows. In Sec. II, we work out the structure of the spin-dependent terms in a convenient basis. We specify the form of the spin-dependent potentials at short distances in Sec. III A, at long distances in Sec. III B, and the interpolation we use in Sec. III C. In Sec. IV, we fix our free parameters using hybrid charmonium lattice data for the lower multiplets and obtain the HFS of higher multiplets. In Sec. V, we obtain the HFS of bottomonium hybrids. Section VI is devoted to the comparison with other approaches, and we close with a discussion and our conclusions in Sec. VII.

II. THE HYPERFINE SPLITTINGS

General expressions for the BOEFT at NLO have been recently obtained in Ref. [7]. The lower-lying hybrid potentials correspond to the $\kappa^p = 1^+$ quantum numbers of the light degrees of freedom (LDOF), where κ is the total angular momentum and p the parity. We focus on the heavy quark spin-dependent terms in the Hamiltonian $V^{(1)}_{\kappa^p}(\mathbf{r})/m_Q$:

$$V^{(1)}_{\kappa^p}(\mathbf{r}) = \sum_{\Lambda\Lambda'} \mathcal{P}_{\kappa\Lambda}[V^{sa}_{\kappa^p\Lambda\Lambda'}(r)\boldsymbol{S}_{Q\bar{Q}}\cdot(\mathcal{P}_{10}\cdot\boldsymbol{S}_\kappa) + V^{sb}_{\kappa^p\Lambda\Lambda'}(r)\boldsymbol{S}_{Q\bar{Q}}\cdot(\mathcal{P}_{11}\cdot\boldsymbol{S}_\kappa)]\mathcal{P}_{\kappa\Lambda'}, \quad (1)$$

where $\boldsymbol{S}_{Q\bar{Q}}$ and $\boldsymbol{S}_\kappa$ are the spin operators of the heavy quark-antiquark pair and the total angular momentum operator of the LDOF, respectively. $\mathcal{P}_{\kappa\Lambda}$ are the projectors to the irreducible representations of the $D_{\infty h}$ group $\Lambda = 0, 1$. They read

$$\mathcal{P}_{10} = \mathbb{I}_3 - (\hat{\boldsymbol{r}}\cdot\boldsymbol{S}_1)^2,$$
$$\mathcal{P}_{11} = (\hat{\boldsymbol{r}}\cdot\boldsymbol{S}_1)^2. \quad (2)$$

In our case, the above potentials act on fields $H_1^{nm}(\mathbf{r},t)$, $n,m = 1,2,3$, where the first index corresponds to the total angular momentum of the LDOF and the second to the spin of the heavy quark-antiquark pair. In the Cartesian basis $(\boldsymbol{S}_1^i)^{jk} = -i\epsilon^{ijk}$, we then have

$$\mathcal{P}_{10}^{n'n} = \hat{r}^{n'}\hat{r}^n,$$
$$\mathcal{P}_{11}^{n'n} = \delta^{n'n} - \hat{r}^{n'}\hat{r}^n. \quad (3)$$

Analogously, the heavy quark-antiquark spin operators read $(\boldsymbol{S}^i_{Q\bar{Q}})^{m'm} = -i\epsilon_{im'm}$. We find that only two independent potentials survive:

$$\begin{aligned}[V^{(1)}_{\kappa^p}(\boldsymbol{r})]^{n'm';nm} &= -V^{sa}_{1^+11}(r)(\delta^{n'm}\delta^{nm'} - \delta^{n'm'}\delta^{nm}) + (V^{sa}_{1^+11}(r) + V^{sb}_{1^+10}(r))\hat{r}^i\hat{r}^j(\delta^{jm}\delta^{n'i}\delta^{nm'} \\ &\quad + \delta^{ni}\delta^{jm'}\delta^{n'm} - \delta^{jm'}\delta^{n'i}\delta^{nm} - \delta^{ni}\delta^{jm}\delta^{n'm'}) \\ &= -2V_{hf}(r)(\delta^{n'm}\delta^{nm'} - \delta^{n'm'}\delta^{nm}) - 2V_{hf2}(r)\left(\hat{r}^i\hat{r}^j - \frac{\delta^{ij}}{3}\right)(\delta^{jm}\delta^{n'i}\delta^{nm'} \\ &\quad + \delta^{ni}\delta^{jm'}\delta^{n'm} - \delta^{jm'}\delta^{n'i}\delta^{nm} - \delta^{ni}\delta^{jm}\delta^{n'm'}), \end{aligned} \quad (4)$$

where we have used that time reversal and Hermiticity imply $V^{sb}_{1^+01}(r) = V^{sb}_{1^+10}(r) \in \mathbb{R}$ and we have defined

$$V_{hf}(r) = \frac{1}{6}V^{sa}_{1^+11}(r) - \frac{1}{3}V^{sb}_{1^+10}(r),$$
$$V_{hf2}(r) = -\frac{1}{2}(V^{sa}_{1^+11}(r) + V^{sb}_{1^+10}(r)). \quad (5)$$

The structure leading to V_{hf} was first noticed in Ref. [4], and the one leading to V_{hf2} was already considered in the short-distance analysis in Refs. [6,21]. We write the field $H_1^{nm}(\mathbf{r},t)$ in the $|SLJ\mathcal{J}\mathcal{M}>$ basis, where S and L are the spin and the orbital angular momentum of the $Q\bar{Q}$ pair, respectively, J the total angular momentum of the LDOF plus the orbital angular momentum of the $Q\bar{Q}$, and $\mathcal{J}$ and $\mathcal{M}$ the total angular momentum and its third component, respectively [4]. For a given $\mathcal{J}$, $J = \mathcal{J}$, $\mathcal{J}\pm1$, $L = J$, $J\pm1$ and only $S = 1$ is affected by Eq. (1):

$$H_1^{ji}(\mathbf{r},t) = \frac{1}{r}\sum_{LJ\mathcal{J}\mathcal{M}} Y^{jiLJ}_{\mathcal{J}\mathcal{M}}(\hat{\mathbf{r}})P^{LJ}_{1\mathcal{J}\mathcal{M}}(r)e^{-iEt}, \quad (6)$$

$$Y^{ijLJ}_{\mathcal{J}M}(\hat{\mathbf{r}}) = \sum_{\mu,\nu=0,\pm1} C(J1\mathcal{J};\mathcal{M}-\nu\nu) \times C(L1J;\mathcal{M}-\mu-\nu\mu)Y_L^{M-\mu}(\hat{\mathbf{r}})\chi^i_\mu\chi^j_\nu, \quad (7)$$

where $C(JJ'J'';MM')$ are Clebsch-Gordan coefficients, $Y_L^M(\hat{\mathbf{r}})$ the spherical harmonics, and χ^i_μ the spin 1 eigenvectors. In this basis, Eq. (1) becomes, for $\mathcal{J} > 1$, a 9×9 matrix that splits into a 5×5 box and a 4×4 box.

The five-dimensional box corresponds to the subspace spanned by $(P^{--}_{1\mathcal{J}\mathcal{M}}, P^{+-}_{1\mathcal{J}\mathcal{M}}, P^{00}_{1\mathcal{J}\mathcal{M}}, P^{-+}_{1\mathcal{J}\mathcal{M}}, P^{++}_{1\mathcal{J}\mathcal{M}})$, where we

use the shorthand notation $\pm$ for $J \pm 1$ or $\mathcal{J} \pm 1$ and 0 for J or $\mathcal{J}$. For the terms proportional to $-2V_{hf}$, it reads [5,22]

$$\begin{pmatrix} 1 & 0 & 0 & 0 & 0 \\ 0 & -\frac{\mathcal{J}-1}{\mathcal{J}} & \frac{\mathcal{J}+1}{\mathcal{J}}\frac{\sqrt{2\mathcal{J}-1}}{\sqrt{2\mathcal{J}+1}} & 0 & 0 \\ 0 & \frac{\mathcal{J}+1}{\mathcal{J}}\frac{\sqrt{2\mathcal{J}-1}}{\sqrt{2\mathcal{J}+1}} & -\frac{1}{\mathcal{J}(\mathcal{J}+1)} & \frac{\mathcal{J}}{\mathcal{J}+1}\frac{\sqrt{2\mathcal{J}+3}}{\sqrt{2\mathcal{J}+1}} & 0 \\ 0 & 0 & \frac{\mathcal{J}}{\mathcal{J}+1}\frac{\sqrt{2\mathcal{J}+3}}{\sqrt{2\mathcal{J}+1}} & -\frac{\mathcal{J}+2}{\mathcal{J}+1} & 0 \\ 0 & 0 & 0 & 0 & 1 \end{pmatrix} \tag{8}$$

and for terms proportional to $-2V_{hf2}$ [23]

$$\begin{pmatrix} \frac{2(2-\mathcal{J})}{-3+6\mathcal{J}} & V_2^{--} & V_2^{-0} & 0 & 0 \\ V_2^{--} & \frac{2(1-\mathcal{J}^2)}{3\mathcal{J}-6\mathcal{J}^2} & V_2^{+-} & 0 & 0 \\ V_2^{-0} & V_2^{+-} & -\frac{2}{3\mathcal{J}(1+\mathcal{J})} & V_2^{00} & V_2^{+0} \\ 0 & 0 & V_2^{00} & \frac{2\mathcal{J}(2+\mathcal{J})}{9+15\mathcal{J}+6\mathcal{J}^2} & V_2^{-+} \\ 0 & 0 & V_2^{+0} & V_2^{-+} & -\frac{2(3+\mathcal{J})}{9+6\mathcal{J}} \end{pmatrix} \tag{9}$$

with

$$V_2^{-0} = \frac{\mathcal{J}+1}{\mathcal{J}(2\mathcal{J}-1)(2\mathcal{J}+1)},$$
$$V_2^{--} = \frac{3\mathcal{J}-2}{2(2\mathcal{J}-1)\sqrt{\mathcal{J}(\mathcal{J}-1)}},$$
$$V_2^{+-} = \frac{\mathcal{J}^2-\mathcal{J}-2}{3\mathcal{J}\sqrt{4\mathcal{J}^2-1}},$$
$$V_2^{00} = \frac{\mathcal{J}(\mathcal{J}+3)}{3(\mathcal{J}+1)\sqrt{4\mathcal{J}(\mathcal{J}+2)+3}},$$
$$V_2^{-+} = -\frac{\sqrt{2+\mathcal{J}}}{(3+2\mathcal{J})\sqrt{1+\mathcal{J}}},$$
$$V_2^{+0} = \mathcal{J}\sqrt{\frac{(2+\mathcal{J})}{(1+\mathcal{J})(1+2\mathcal{J})(3+2\mathcal{J})}}.$$

The four-dimensional box corresponds to the subspace spanned by $(P^{0-}_{1\mathcal{J}\mathcal{M}}, P^{-0}_{1\mathcal{J}\mathcal{M}}, P^{+0}_{1\mathcal{J}\mathcal{M}}, P^{0+}_{1\mathcal{J}\mathcal{M}})$. For the terms proportional to $-2V_{hf}$, it reads [5,22]

$$\begin{pmatrix} \frac{1}{\mathcal{J}} & \frac{\sqrt{\mathcal{J}^2-1}}{\mathcal{J}} & 0 & 0 \\ \frac{\sqrt{\mathcal{J}^2-1}}{\mathcal{J}} & -\frac{1}{\mathcal{J}} & 0 & 0 \\ 0 & 0 & \frac{1}{\mathcal{J}+1} & \frac{\sqrt{(\mathcal{J}+2)\mathcal{J}}}{\mathcal{J}} \\ 0 & 0 & \frac{\sqrt{(\mathcal{J}+2)\mathcal{J}}}{\mathcal{J}} & -\frac{1}{\mathcal{J}+1} \end{pmatrix} \tag{10}$$

and for terms proportional to $-2V_{hf2}$ [23]

$$\begin{pmatrix} \frac{2}{3\mathcal{J}} & V_2^{0--0} & V_2^{0-+0} & 0 \\ V_2^{0--0} & -\frac{2}{3\mathcal{J}}+\frac{2}{1+2\mathcal{J}} & V_2^{-0+0} & \frac{\mathcal{J}\sqrt{1+\frac{1}{1+\mathcal{J}}}}{1+2\mathcal{J}} \\ V_2^{0-+0} & V_2^{-0+0} & -\frac{2(2+\mathcal{J})}{3+9\mathcal{J}+6\mathcal{J}^2} & V_2^{+00+} \\ 0 & \frac{\mathcal{J}\sqrt{1+\frac{1}{1+\mathcal{J}}}}{1+2\mathcal{J}} & V_2^{+00+} & -\frac{2}{3+3\mathcal{J}} \end{pmatrix} \tag{11}$$

with

$$V_2^{0--0} = \frac{\sqrt{\mathcal{J}^2-1}}{3\mathcal{J}} + \frac{\sqrt{\frac{\mathcal{J}-1}{\mathcal{J}}}(1+\mathcal{J})}{1+2\mathcal{J}},$$
$$V_2^{0-+0} = \frac{(1+\mathcal{J})\sqrt{1-\frac{2}{1+2\mathcal{J}}}}{3\mathcal{J}},$$
$$V_2^{-0+0} = \frac{\sqrt{\frac{\mathcal{J}}{1+\mathcal{J}}}-\sqrt{\frac{\mathcal{J}+1}{\mathcal{J}}}}{1+2\mathcal{J}},$$
$$V_2^{+00+} = \frac{\sqrt{\mathcal{J}(2+\mathcal{J})}(\mathcal{J}-1)}{3(\mathcal{J}+1)(2\mathcal{J}+1)}.$$

If $\mathcal{J}=1$, $P^{--}_{1\mathcal{J}\mathcal{M}}$ and $P^{0-}_{1\mathcal{J}\mathcal{M}}$ do not exist and the matrices are 7×7. If $J=0$, $P^{--}_{1\mathcal{J}\mathcal{M}}$, $P^{+-}_{1\mathcal{J}\mathcal{M}}$, $P^{00}_{1\mathcal{J}\mathcal{M}}$, $P^{0-}_{1\mathcal{J}\mathcal{M}}$, $P^{-0}_{1\mathcal{J}\mathcal{M}}$, and $P^{+0}_{1\mathcal{J}\mathcal{M}}$ do not exist and the system is reduced to 3×3 matrices for both potentials.

At first order in perturbation theory, only the diagonal terms and the off-diagonal terms corresponding to $L=J\pm 1, L'=J\mp 1$ matter. This is because the 0th-order wave functions have a single component for $L=J$ and two components for $L=J\pm 1$. Then the following formulas for the masses $M_{S\mathcal{J}}$ of the spin multiplet J, which are independent of the potentials V_{hf} and V_{hf2}, hold:

$$\frac{M_{1J+1}-M_{0J}}{M_{1J}-M_{0J}} = -J, \qquad \frac{M_{1J-1}-M_{0J}}{M_{1J}-M_{0J}} = J+1. \tag{12}$$

They were initially derived in Refs. [5,22] for $V_{hf2}=0$, but it is not difficult to see that they are also fulfilled for $V_{hf2}\neq 0$ [23].

III. THE POTENTIALS

The potentials $V^{sa}_{1^+11}(r)$ and $V^{sb}_{1^+10}(r)$ can be obtained from suitable operator insertions in the expectation values of Wilson loops [7], and, hence, they are amenable to lattice evaluations. However, no such evaluation exists to date. The short-distance behavior can be worked out with the help of potential non-relativistic QCD (pNRQCD) [24,25]. It has been obtained at NLO in the $1/m_Q$ expansion in Refs. [6,15]. However, the typical distances at which the static hybrid potentials reach the minimum [26–29], the typical quark-antiquark distance in the bound states [3], and the shape of the wave functions (see plots in Sec. VI in Ref. [4]) indicate that most of the time the quark-antiquark

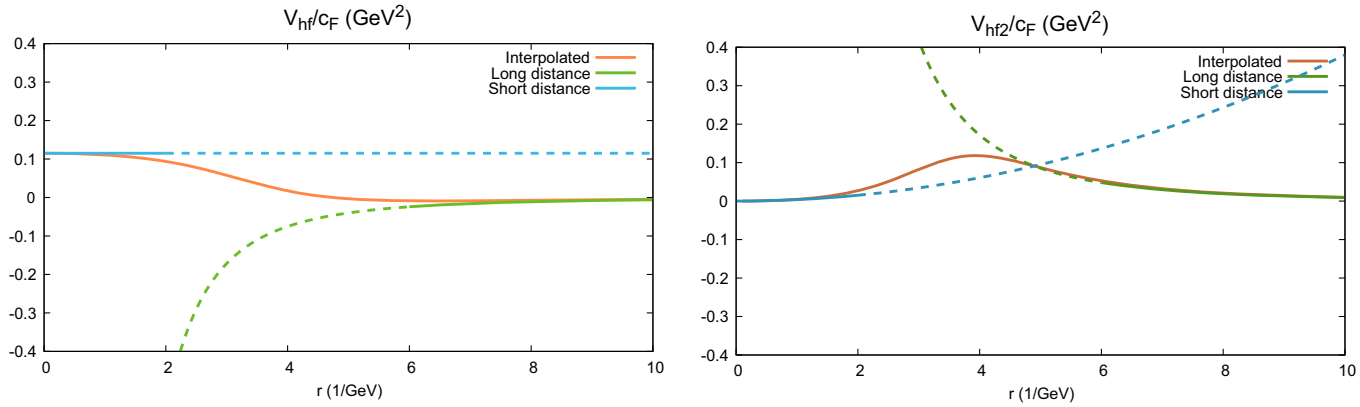

FIG. 1. The two spin-dependent potentials (5) at short (13) [blue line] and long (14) [green line] distances. The orange line shows the interpolation we use (16). The short-distance parameters A and B correspond to those in Table III and $r_0 = 3.96$ GeV^{-1}.

separation is of the order of $1/\Lambda_{\rm QCD}$. It may then be more appropriate incorporating reliable long-distance information rather than calculating higher orders at short distances. We shall do that by using the effective string theory of QCD [16,30], which describes well the long-distance behavior of the static hybrid potentials [26], as well as those of the $1/m_Q$ and $1/m_Q^2$ potentials for quarkonium [4,18], calculated in lattice $SU(3)$ pure Yang-Mills theory. We will then stick to the Cornell model's philosophy of using potentials that interpolate between known short- and long-distance behavior.

A. The short-distance behavior

In order to estimate the short-distance behavior, we use the fact that the $1/m_Q$ potentials are analytic in $\mathbf{r}$ in pNRQCD. This implies that

$$V_{hf}(r)/m_Q = A + \mathcal{O}(r^2),$$
$$V_{hf2}(r)/m_Q = Br^2 + \mathcal{O}(r^4). \tag{13}$$

We shall keep the LO terms only. A and B are unknown real constants: $A = c_F k_A/m_Q$ and $B = c_F k_B/m_Q$. $k_A \sim \Lambda_{\rm QCD}^2$ and $k_B \sim \Lambda_{\rm QCD}^4$ can be related to expectation values of operator insertions in Wilson lines [15]. $c_F = c_F(m_Q)$ is a short-distance matching coefficient inherited from NRQCD [31–33]. We shall take the next-to-leading logarithmic expression for it, $c_F(m_b) \equiv c_F(\nu = 1\ \text{GeV}, m_c) = 1.12155$ and $c_F(m_b) \equiv c_F(\nu = 1\ \text{GeV}, m_b) = 0.87897$. The corrections to the leading short-distance behavior are suppressed by powers of $\Lambda_{\rm QCD}^2 r^2$. We display the potentials (13) in Fig. 1.

B. The long-distance behavior

The long-distance behavior can be estimated using the QCD effective string theory [16,17], following the mapping given in Ref. [18]. It has been obtained in Ref. [34]; see the Appendix:

$$\frac{V^{sa}_{1^+11}(r)}{m_Q} = -\frac{2c_F\pi^2 g\Lambda'''}{m_Q \kappa r^3} \equiv V^{sa}_{ld}(r),$$
$$\frac{V^{sb}_{1^+10}(r)}{m_Q} = \mp\frac{c_F g\Lambda'\pi^2}{m_Q\sqrt{\pi\kappa}}\frac{1}{r^2} \equiv V^{sb}_{ld}(r). \tag{14}$$

The parameters $g\Lambda' \sim \Lambda_{\rm QCD}$ and $g\Lambda''' \sim \Lambda_{\rm QCD}$ also appear in the spin-dependent potentials for heavy quarkonium. They have been obtained in Ref. [4] from the lattice data in Refs. [35,36]. Using simple interpolations with the right short- and long-distance behavior, a good fit to data is obtained with the following outcome[1]:

$$g\Lambda' \sim -59\ \text{MeV}, \qquad g\Lambda''' \sim \pm 230\ \text{MeV}. \tag{15}$$

If only long-distance data points and the long-distance form of the potentials are used, the values of $|g\Lambda'|$ and $|g\Lambda'''|$ are 40% and 35% larger, respectively. $\kappa \simeq 0.187$ GeV^2 is the string tension, and c_F is the same NRQCD matching coefficient that appears in the short-distance behavior. The corrections to the leading long-distance behavior of the potentials in Eq. (14) are suppressed by factors $1/r^2\Lambda_{\rm QCD}^2$. We display the potentials (5) at long distances in Fig. 1.

C. The interpolating potentials

We use for the hyperfine potentials simple interpolations with the right short- and long-distance behavior obtained in Secs. III A and III B, respectively:

$$\frac{V_{hf}(r)}{m_Q} = \frac{A + \left(\frac{r}{r_0}\right)^2\left(\frac{1}{6}V^{sa}_{ld}(r_0) - \frac{r}{3r_0}V^{sb}_{ld}(r_0)\right)}{1 + \left(\frac{r}{r_0}\right)^5},$$
$$\frac{V_{hf2}(r)}{m_Q} = \frac{Br^2 - \left(\frac{r}{r_0}\right)^5\left(\frac{r_0}{2r}V^{sa}_{ld}(r_0) + \frac{1}{2}V^{sb}_{ld}(r_0)\right)}{1 + \left(\frac{r}{r_0}\right)^7}. \tag{16}$$

[1]This is so except for the spin-spin potential, which was not used for the extraction of $g\Lambda'$ and $g\Lambda'''$ in Ref. [4].

$g\Lambda'''$ is the matching scale. It is estimated from the short- and long-distance behavior of the static hybrid potentials to be $r_0 \simeq 3.96\ \mathrm{GeV}^{-1}$. This figure will be eventually moved in order to estimate the error due to the interpolation dependence. We show the interpolated potentials in Fig. 1.

IV. CHARMONIUM HYBRIDS: FIXING THE SHORT-DISTANCE PARAMETERS

The short-distance potentials depend on two arbitrary parameters at LO: A and B. We shall fix those parameters by comparing our results to the lattice data in Ref. [20] for the lower-lying hybrid states [the $1(s/d)_1$ (H_1), $1p_1$ (H_2), $1(p/f)_2$ (H_4), and $1p_0$ (H_3) multiplets]. The spin average of the multiplets in Ref. [20] was higher than in Ref. [4]. Since we are going to use the same methodology as in the last reference, we correct the lattice data by the spin average difference, namely, by 381 [$1(s/d)_1$], 326 ($1p_1$), 392 [$1(p/f)_2$], and 151 ($1p_0$) MeV. We then scan natural values of A and B in $[-0.3, 0.3]$ GeV and $[-0.06, 0.06]$ GeV^3, respectively, and search for the ones with the lowest χ^2/d.o.f. We adapted the code used in Ref. [4] by adding the spin-dependent potentials above and neglecting, for simplicity, the mixing with quarkonium [37]. The charm mass is also taken as in Ref. [4]: $m_c = 1.47\,\mathrm{GeV}$. If we neglect the long-distance behavior, we find $A = 0.0699\,\mathrm{GeV}$ and $B = 0.0008\,\mathrm{GeV}^3$ with $\chi^2/\mathrm{d.o.f.} = 1.1927$. When we include the long-distance behavior, the fit quality improves considerably, and we obtain as a best fit $A = 0.1356$ GeV and $B = -0.0022$ GeV^3 with $\chi^2/\mathrm{d.o.f.} = 0,\ 6439$. $g\Lambda'$ and $g\Lambda'''$ are taken as in Eq. (15), $r_0 = 3.96\ \mathrm{GeV}^{-1}$ in Eq. (16), and all possible sign combinations for the long-distance potentials in Eqs. (14) and (15) are considered. The best fit corresponds to a negative $V_{ld}^{sa}(r)$ and a positive $V_{ld}^{sb}(r)$. The former implies $g\Lambda''' < 0$. Reversing the sign of $V_{ld}^{sa}(r)$ [$V_{ld}^{sb}(r)$] worsens the fit considerably (marginally); see Table I.

We have also explored the dependence of the result on $g\Lambda'$ and $g\Lambda'''$ according to the possible values given in Ref. [4]. The fit has a mild preference for larger values of $|g\Lambda'|$ and $|g\Lambda'''|$ ($\chi^2/\mathrm{d.o.f.} = 0, 632$ versus $\chi^2/\mathrm{d.o.f.} = 0, 643$), so we shall take for now on $g\Lambda' = -0.0796$ GeV and $g\Lambda''' = 0.3105$ GeV, which correspond to the fit to long-distance data only in Ref. [4]. These values lead to $A = 0.1445$ GeV and $B = -0.0036$ GeV^3. The change in the spectrum is negligibly small ($\lesssim 1$ MeV). The interpolation dependence is estimated by moving $r_0 \in [2.5, 5]\ \mathrm{GeV}^{-1}$. The χ^2/d.o.f. marginally improves around $r_0 \sim 3.5\ \mathrm{GeV}^{-1}$ and considerably deteriorates for $r_0 \leq 3\ \mathrm{GeV}^{-1}$ and $r_0 > 3.96\ \mathrm{GeV}^{-1}$. We shall stick to the default value $r_0 = 3.96\ \mathrm{GeV}^{-1}$ and use $r_0 \sim 3.5\ \mathrm{GeV}^{-1}$ to estimate the error due to the interpolation. The changes in the spectrum are of 3.1 MeV in average, with a maximum of 7 MeV.

TABLE I. Fit parameters and spectrum dependence on the sign ambiguities arising from the long-distance spin-dependent potentials.

Sign(V_{ld}^{sq}) sign(V_{ld}^{sb})		+−	++	−+	−−
χ^2/d.o.f.		0.8323	0.7524	0.6439	0.6850
A (GeV)		0.0764	0.0873	0.1356	0.1256
B(GeV^3)		0.0120	0.0144	−0.0022	−0.0045
$(s/d)_1$ mass (GeV)	1^{--}	4.0107	4.0107	4.0107	4.0107
	0^{-+}	3.9059	3.9029	3.8959	3.8988
	1^{-+}	3.9582	3.9569	3.9548	3.9558
	2^{-+}	4.0597	4.0603	4.0612	4.0611
p_1 mass (GeV)	1^{++}	4.1450	4.1450	4.1450	4.1450
	0^{+-}	4.0886	4.0904	4.0981	4.0955
	1^{+-}	4.0880	4.0921	4.1020	4.0984
	2^{+-}	4.1456	4.1467	4.1495	4.1485
$(p/f)_2$ mass (GeV)	2^{++}	4.2316	4.2316	4.2316	4.2316
	1^{+-}	4.1963	4.1969	4.1959	4.1950
	2^{+-}	4.2366	4.2343	4.2323	4.2343
	3^{+-}	4.2660	4.2637	4.2569	4.2594
p_0 mass (GeV)	0^{++}	4.4864	4.4864	4.4864	4.4864
	1^{+-}	4.4674	4.4693	4.4564	4.4554

A increases about 30%, and B becomes more than twice its value. See Table II.

In order to establish the error of A and B due to the input data, we assume a linear dependence of the binding energy on them, which holds at first order in perturbation theory. We obtain $A = 0.115 \pm 0.034$ GeV and $B = 0.0038 \pm 0.0154$ GeV^3. Notice that the value of B is compatible with zero. The spectrum is displayed in Table III. The error due to the uncertainty in $g\Lambda'$ and $g\Lambda'''$ is negligible. We also neglect the error due to the interpolation, which is not

TABLE II. Fit parameters and spectrum dependence on r_0.

r_0 (GeV^{-1})		2.5	3	3.5	3.96	5
χ^2/d.o.f.		1.0693	0.7088	0.6216	0.6318	0.7585
A (GeV)		0.3718	0.2439	0.1793	0.1445	0.1049
B (GeV^3)		−0.0906	−0.0251	−0.0089	−0.0036	−0.0001
$(s/d)_1$ mass	1^{--}	4.0107	4.0107	4.0107	4.0107	4.0107
(GeV)	0^{-+}	3.8765	3.8836	3.8894	3.8945	3.9038
	1^{-+}	3.9547	3.9525	3.9529	3.9543	3.9578
	2^{-+}	4.0438	4.0543	4.0593	4.0609	4.0604
p_1 mass	1^{++}	4.1450	4.1450	4.1450	4.1450	4.1450
(GeV)	0^{+-}	4.1122	4.1021	4.0991	4.0974	4.0946
	1^{+-}	4.1172	4.1174	4.1119	4.1045	4.0927
	2^{+-}	4.1559	4.1550	4.1524	4.1502	4.1471
$(p/f)_2$ mass	2^{++}	4.2316	4.2316	4.2316	4.2316	4.2316
(GeV)	1^{+-}	4.2291	4.2073	4.1975	4.1952	4.1958
	2^{+-}	4.2334	4.2319	4.2320	4.2327	4.2349
	3^{+-}	4.2226	4.2366	4.2474	4.2545	4.2633
p_0 mass	0^{++}	4.4864	4.4864	4.4864	4.4864	4.4864
(GeV)	1^{+-}	4.4640	4.4558	4.4534	4.4546	4.4597

TABLE III. Fit errors in A, B, and the hybrid charmonium spectrum. The total errors in the spectrum are obtained by adding in quadrature to the fit errors the error due to missing higher orders in the $1/m_Q$ expansion ($\sim\Lambda_{\rm QCD}^3/m_Q^2 \sim 30$ MeV).

			Fit error	Total error
A (GeV)		0.11455	0.034	
B (GeV^3)		0.00385	0.0154	
$(s/d)_1$ mass (GeV)	1^{--}	4.011		0.030
	0^{-+}	3.911	0.045	0.054
	1^{-+}	3.963	0.023	0.038
	2^{-+}	4.046	0.018	0.035
p_1 mass (GeV)	1^{++}	4.145		0.030
	0^{+-}	4.087	0.054	0.061
	1^{+-}	4.055	0.023	0.037
	2^{+-}	4.130	0.005	0.030
$(p/f)_2$ mass (GeV)	2^{++}	4.232		0.030
	1^{+-}	4.235	0.019	0.035
	2^{+-}	4.258	0.021	0.037
	3^{+-}	4.241	0.013	0.033
p_0 mass (GeV)	0^{++}	4.486		0.030
	1^{+-}	4.450	0.013	0.033

negligible in order to obtain a value for A and B, but it is for the spectrum due to its correlation with $r0$. We include the error due to higher orders in the $1/m_Q$ expansion, which is about 30 MeV for charm.

In Ref. [4], it was found that two extra multiplets lie below the $1p_0$: the $2(s/d)_2$ and the d_2. For completeness, we also display the spectrum of these multiplets including the hyperfine splitting in Table IV.

V. BOTTOMONIUM HYBRIDS: PREDICTING THE HYPERFINE SPLITTINGS

Once the parameters A and B are fixed from charmonium, the corresponding parameters for bottomonium, A' and B', also are:

TABLE IV. The remaining hybrid charmonium spectrum below the $1p_0$ multiplet. The total errors in the spectrum are obtained by adding in quadrature to the errors induced by the uncertainties in A and B the error due to missing higher orders in the $1/m_Q$ expansion ($\sim\Lambda_{\rm QCD}^3/m_Q^2 \sim 30$ MeV).

		Mass (GeV)	A and B error	Total error
d_2	2^{--}	4.486		0.030
	1^{-+}	4.287	$^{+0.050}_{-0.062}$	$^{+0.059}_{-0.068}$
	2^{-+}	4.302	$^{+0.031}_{-0.039}$	$^{+0.043}_{-0.049}$
	3^{-+}	4.333	$^{+0.003}_{-0.034}$	$^{+0.030}_{-0.046}$
$2(s/d)_1$	1^{--}	4.355		0.030
	0^{-+}	4.280	$^{+0.060}_{-0.066}$	$^{+0.067}_{-0.072}$
	1^{-+}	4.334	$^{+0.020}_{-0.006}$	$^{+0.036}_{-0.031}$
	2^{-+}	4.394	$^{+0.013}_{-0.032}$	$^{+0.033}_{-0.044}$

$$A' = A\frac{c_F(m_b)m_c}{c_F(m_c)m_b}, \qquad B' = B\frac{c_F(m_b)m_c}{c_F(m_c)m_b}. \quad (17)$$

We calculate the spectrum for the central values of these parameters ($A' = 0.02704$ GeV and $B' = 0.00091$ GeV^3), which provides us with the central value of the masses, and for the four corners of their 1σ range, which allows us to estimate the error due to the fit parameters. We take it as the larger difference in either sense. The total error is obtained by adding in quadrature to the latter the error associated to higher orders $\sim\Lambda_{\rm QCD}^3/m_Q^2 \sim 3$ MeV. The bottom mass is taken as in Ref. [4]: $m_b = 4.88$ GeV. We display the results in Table V.

We have also explored the dependence on r_0. We have recalculated the central values for $r_0 = 3.5$ GeV^{-1} and the corresponding parameters [obtained from charm and

TABLE V. The hybrid bottomonium spectrum. The total errors in the spectrum are obtained by adding in quadrature to the fit errors the error due to missing higher orders in the $1/m_Q$ expansion ($\sim\Lambda_{\rm QCD}^3/m_Q^2 \sim 3$ MeV).

		Mass (GeV)	A and B error	Total error
$(s/d)_1$	1^{--}	10.6902		0.003
	0^{-+}	10.682	0.004	0.005
	1^{-+}	10.686	0.002	0.004
	2^{-+}	10.694	0.002	0.003
p_1	1^{++}	10.761		0.003
	0^{+-}	10.756	0.004	0.005
	1^{+-}	10.759	0.002	0.004
	2^{+-}	10.764	0.002	0.003
$(p/f)_2$	2^{++}	10.819		0.003
	1^{+-}	10.815	0.002	0.003
	2^{+-}	10.818	0.000	0.003
	3^{+-}	10.821	0.001	0.003
d_2	2^{--}	10.870		0.003
	1^{-+}	10.869	$^{+0.001}_{-0.003}$	$^{+0.003}_{-0.005}$
	2^{-+}	10.869	$^{+0.001}_{-0.002}$	$^{+0.003}_{-0.004}$
	3^{-+}	10.871	0.001	0.003
$2(s/d)_1$	1^{--}	10.885		0.003
	0^{-+}	10.881	$^{+0.002}_{-0.005}$	$^{+0.004}_{-0.006}$
	1^{-+}	10.883	$^{+0.001}_{-0.002}$	0.003
	2^{-+}	10.888	$^{+0.003}_{-0.001}$	$^{+0.004}_{-0.003}$
$2p_1$	1^{++}	10.970		0.003
	0^{+-}	10.967	$^{+0.002}_{-0.004}$	$^{+0.005}_{-0.004}$
	1^{+-}	10.968	$^{+0.002}_{-0.001}$	$^{+0.004}_{-0.003}$
	2^{+-}	10.971	0.001	0.003
$2(p/f)_2$	2^{++}	11.005		0.003
	1^{+-}	11.003	$^{+0.001}_{-0.002}$	0.003
	2^{+-}	11.005	0.000	0.003
	3^{+-}	11.007	0.001	0.003
p_0	0^{++}	11.012		0.003
	1^{+-}	11.012	0.000	0.003

converted to bottom according to Eq. (17), $A' = 0.0423$ GeV and $B' = -0.0021$ GeV^3]. Recall that this r_0 choice provides a slightly better fit to charmonium lattice data than our default $r_0 = 3.96$ GeV^{-1}. The difference is below 1 MeV for the $(s/d)_1$ multiplet and around 0.1 MeV for the remaining ones. We can then safely neglect it.

VI. COMPARISON WITH OTHER APPROACHES

We shall compare here our results with those also obtained in BOEFT in Refs. [6,15] and with the lattice QCD results of the HSC Collaboration [20,38] (we will not use earlier results at larger pion masses [39]). Recall that the main differences with respect to Refs. [6,15] is that only short-distance expressions for the spin-dependent potentials at NLO (eight nonperturbative parameters to fit) are used there, whereas we use LO short-distance expressions and LO long-distance expressions (two nonperturbative parameters to fit).

Lattice results for charmonium hybrids [20] are used to fit the nonperturbative parameters. Hence, our errors are slightly larger than the ones from lattice data. Our fits have lower χ^2/d.o.f. than those in Refs. [6,15], which supports the inclusion of long-distance potentials. The overall picture for the charmonium hyperfine splittings is similar to the one obtained in those references; see Fig. 2.

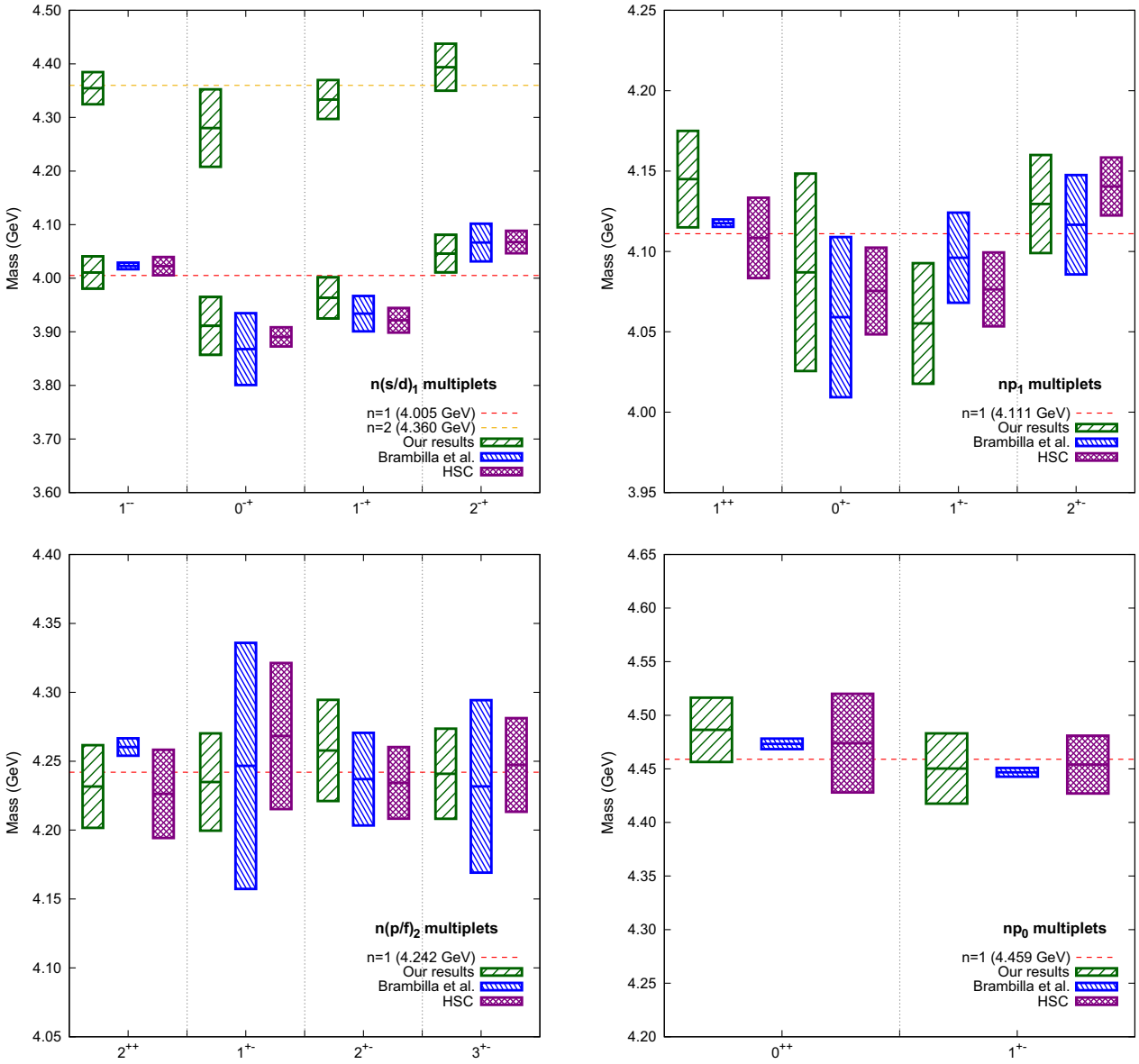

FIG. 2. The spectrum of the lower-lying $n(s/d)_1$ (H_1), np_1 (H_3), $n(p/f)_2$ (H_4), and np_0 (H_3) charmonium hybrids computed by adding the LO spin-dependent potentials to the static potentials used in Ref. [4] is shown in green boxes. The average mass for each multiplet is shown as a red dashed line. Blue and magenta boxes show the results of the BOEFT with NLO spin-dependent short-distance potentials only [6,15] and lattice QCD [20], respectively, adjusted to our spin average. The height of the boxes indicates the uncertainty.

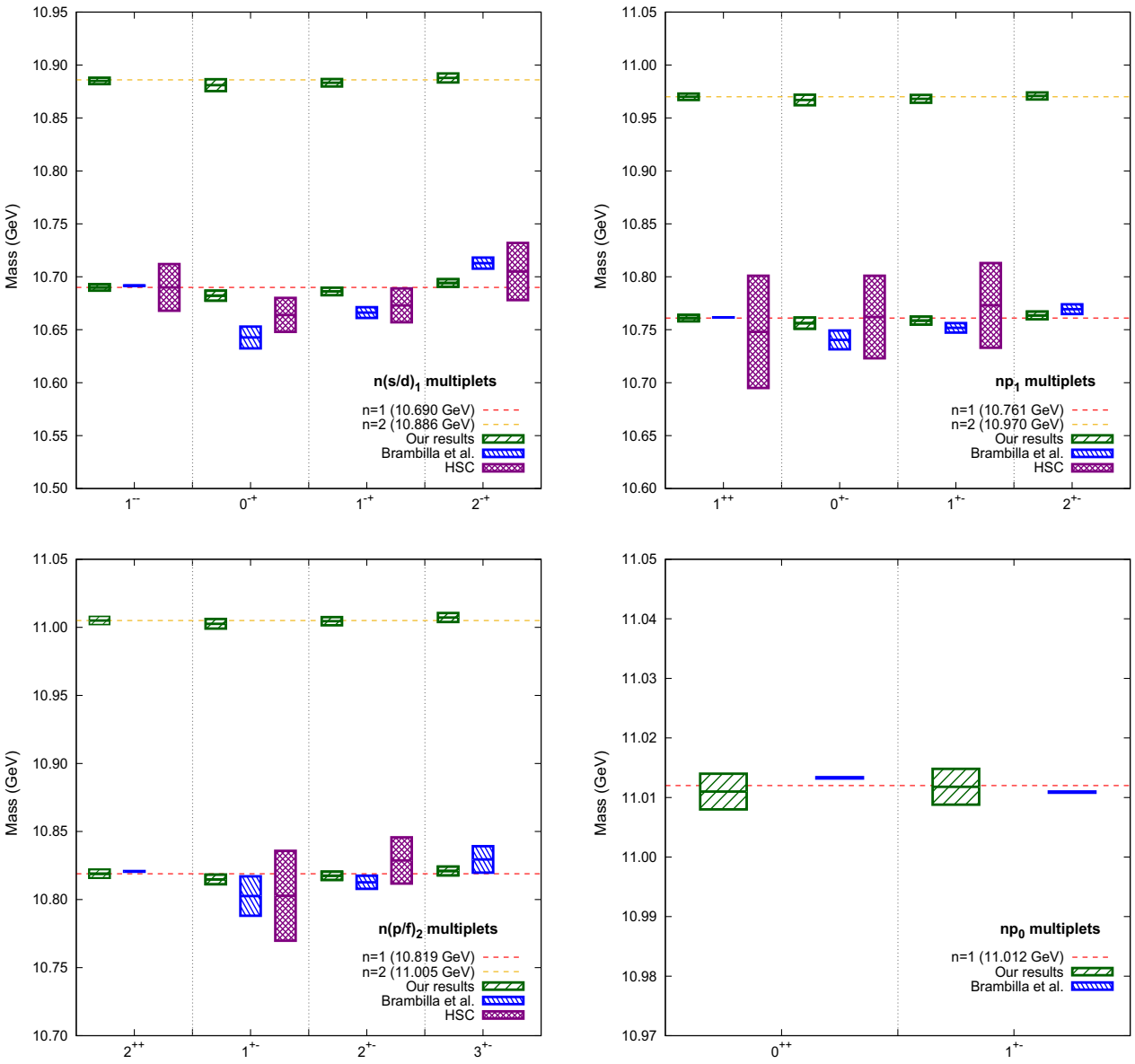

FIG. 3. The spectrum of the lower-lying $n(s/d)_1$ (H_1), np_1 (H_3), $n(p/f)_2$ (H_4), and np_0 (H_3) bottomonium hybrids computed by adding the LO spin-dependent potentials to the static potentials used in Ref. [4] is shown in green boxes. The average mass for each multiplet is shown as a red dashed line. Blue and magenta boxes show the results of the BOEFT with NLO spin-dependent short-distance potentials only [6,15] and lattice QCD [38], respectively, adjusted to our spin average. The height of the boxes indicates the uncertainty.

For spin-one states, we get similar, slightly larger, smaller, and larger errors for the $(s/d)_1$ (H_1), p_1 (H_3), $(p/f)_2$ (H_4), and p_0 (H_3) multiplets, respectively. For spin-zero states, which do not enter in our analysis, the errors are due only to neglected higher orders in the $1/m_Q$ expansion. Note that the error that we assign to them is larger than than the one assigned in Refs. [6,15]. See Fig. 2.

Our predictions for the bottomonium hybrid hyperfine splittings are compatible with the few available states from lattice QCD [38], but we have much smaller errors; see Fig. 3. We get again an overall picture similar to the one in Refs. [6,15], with smaller errors for spin-one states, and smaller hyperfine splittings, in general. However, for the $(s/d)_1$ multiplet, we have about 2σ discrepancies with those references. Nevertheless, both sets of splittings are consistent with lattice data in Ref. [38] for this multiplet. The remaining available lattice states do not form any obvious spin multiplet. We have assigned the three lighter (two heavier) ones to the p_1 $[(p/f)_2]$ multiplet. However, the fact that the 1^{++} state is lighter than the 1^{--} in the lattice results is in conflict with the BOEFT ones.

VII. DISCUSSION AND CONCLUSIONS

The static potentials we use are taken from Ref. [4]. They were obtained from pure $SU(3)$ $(n_f = 0)$ lattice data in

Refs. [26,27]. More recent pure $SU(3)$ ($n_f = 0$) lattice data exist for the static hybrid potentials, with better resolution at short and intermediate distances [28,29,40]. It would be interesting to incorporate them in future analysis. However, the systematic errors due to using pure $SU(3)$ ($n_f = 0$) rather than QCD with dynamical light quarks ($n_f = 3$) would still be difficult to evaluate. The early study in Ref. [41] suggests that they are small. The strategy recently presented in Ref. [42] may help to resolve this issue.

The lattice data to which we fit our spin-dependent expressions (Ref. [20]) are obtained from a $2+1+1$ clover action at a fixed spatial lattice spacing of 0.12 fm, a 3.5 times smaller temporal lattice spacing, and light quark masses corresponding to $m_\pi \sim 240$ MeV. In Ref. [43], results in the continuum limit for realistic light quark masses are obtained using a highly improved staggered quarks action with $2+1+1$ dynamical quarks, but only for two states in the lowest-lying multiplet. The lattice bottomonium data we compare with (Ref. [38]) uses the same setting as Ref. [20], tuning the heavy quark parameters to bottomonium observables, and uses light quark masses corresponding to $m_\pi \sim 391$ MeV.

We have focused on the hyperfine splittings. The absolute values of the masses we quote correspond to the spin averages in Ref. [4]. The central values quoted in that reference are lower than those in Ref. [3] but compatible within errors. The differences are due to the choice of normalization (quarkonium spectrum versus RS mass scheme). They are also much lower than the lattice results in Ref. [20], a difference that shrinks if they are compared with earlier lattice data at larger pion mass [39]. This suggests that part of the discrepancy may be due to the quenched lattice data used as an input in Refs. [3,4]. They are also lower than in most models (see Ref. [44] for a review). Since the discrepancies usually amount to global shifts, they are not expected to affect the bulk of the hyperfine splitting analysis presented here. However, a small dependence on the input lattice data (unphysical) pion mass was noticed in the short-distance analysis of Ref. [15], which may be present in our results as well.

We have shown that the inclusion of long-distance contributions calculated in the QCD EST to the LO spin-dependent potentials in the BOEFT considerably improves the description of the charmonium hybrid hyperfine splittings obtained in lattice QCD [20]. For the LO spin-dependent potentials, the χ^2/d.o.f. moves from 1.193 for short-distance contributions only to 0.644 for short- and long-distance contributions. This figure is much lower than the $\chi^2/\text{d.o.f.} = 0.999$ obtained in Ref. [15] for NLO spin-dependent potential with short-distance contributions only. The fact that long-distance contributions are important may be anticipated from the results on the size of charmonium hybrids displayed in Table III in Ref. [3], $\langle 1/r \rangle \in [190, 420]$ MeV, scales of the order of $\Lambda_{\rm QCD}$. Using the QCD EST to describe them has the remarkable feature that it introduces no new unknown parameter, beyond sign ambiguities and the scale r_0 that separates short and long distances in the interpolation. Hence, we have two parameter fits to data, rather than the eight parameter fits in Ref. [15], leading to a smaller χ^2/d.o.f. as mentioned above.

Once we have the unknown parameters fixed, we can calculate the hyperfine splittings of higher charmonium hybrid states, of the bottomonium ones, and the error associated to them. This is displayed in Tables III–V and in Figs. 2 and 3. For charmonium hybrids, we get results compatible with Ref. [15] with similar errors overall and, as expected, compatible with Ref. [20], the source of our fit, with slightly larger errors. For bottomonium hybrids, our hyperfine splittings are compatible with those in Ref. [38], with much smaller errors, but smaller than those in Ref. [15], with similar errors.

ACKNOWLEDGMENTS

We thank Rubén Oncala for providing us with the code used in Ref. [4] and Jaume Tarrús Castellà and Jorge Segovia for providing us for the data and figures used in Refs. [6,15,21]. J. S. acknowledges financial support from Grants No. 2017-SGR-929 and No. 2021-SGR-249 from the Generalitat de Catalunya and from Projects No. PID2019–105614 GB-C21, No. PID2019–110165 GB-I00, and No. CEX2019-000918-M from Ministerio de Ciencia, Innovación y Universidades. S. T. V. acknowledges financial support from the department's collaboration grant call 2022–2023 bestowed by Ministeri d'Eduació i Formació Professional.

APPENDIX: EFFECTIVE STRING THEORY CALCULATION

The general expressions for the (heavy quark) spin-dependent potentials (1), given in Ref. [7], reduce for $\kappa^p = 1^+$ to

$$\frac{V^{sa}_{1^+11}(r)}{m_Q} = \lim_{T\to\infty} \frac{g c_F}{m_Q T} \int_{-\frac{T}{2}}^{\frac{T}{2}} dt \frac{\langle B^*(\mathbf{0},\frac{T}{2}) B^3(\frac{\mathbf{r}}{2},t) B(\mathbf{0},-\frac{T}{2}) - B(\mathbf{0},\frac{T}{2}) B^3(\frac{\mathbf{r}}{2},t) B^*(\mathbf{0},-\frac{T}{2})\rangle_\square}{\langle B(\mathbf{0},\frac{T}{2}) B^*(\mathbf{0},-\frac{T}{2}) + B^*(\mathbf{0},\frac{T}{2}) B(\mathbf{0},-\frac{T}{2})\rangle_\square},$$
$$\frac{V^{sb}_{1^+10}(r)}{m_Q} = \lim_{T\to\infty} \frac{g c_F}{4 m_Q} \frac{V_{\Pi_u} - V_{\Sigma_u^-}}{\sin((V_{\Pi_u} - V_{\Sigma_u^-})\frac{T}{2})} \int_{-\frac{T}{2}}^{\frac{T}{2}} dt \frac{\langle (B^*(\mathbf{0},\frac{T}{2}) B(\frac{\mathbf{r}}{2},t) - B(\mathbf{0},\frac{T}{2}) B^*(\frac{\mathbf{r}}{2},t)) B^3(\mathbf{0},-\frac{T}{2})\rangle_\square}{\langle B(\mathbf{0},\frac{T}{2}) B^*(\mathbf{0},-\frac{T}{2}) + B^*(\mathbf{0},\frac{T}{2}) B(\mathbf{0},-\frac{T}{2})\rangle_\square^{1/2} \langle B^3(\mathbf{0},\frac{T}{2}) B^3(\mathbf{0},-\frac{T}{2})\rangle_\square^{1/2}}, \quad \text{(A1)}$$

where $B^i(\mathbf{r},t)$, $i=1,2,3$ are the three components of the chromomagnetic field and

$$B(\mathbf{r},t) = B^1(\mathbf{r},t) + iB^2(\mathbf{r},t),$$
$$B^*(\mathbf{r},t) = B^1(\mathbf{r},t) - iB^2(\mathbf{r},t). \tag{A2}$$

$\hat{\mathbf{r}}$ is taken in the z direction. The mapping of the operator insertions in the temporal Wilson lines onto EST operators was given in Ref. [18]:

$$\begin{aligned} B(\pm\mathbf{r}/2,t) &\to -i\sqrt{2}\Lambda'\partial_t\partial_z\varphi(\pm r/2,t),\\ B^*(\pm\mathbf{r}/2,t) &\to i\sqrt{2}\Lambda'\partial_t\partial_z\varphi^*(\pm r/2,t),\\ B^3(\pm\mathbf{r}/2,t) &\to i\Lambda'''\partial_t\partial_z\varphi(\pm r/2,t)\partial_z\varphi^*(\pm r/2,t)\\ &\quad + \text{H.c.}, \end{aligned} \tag{A3}$$

and the mapping of the operator insertions in the middle of spatial Wilson lines at $t=\pm T/2$ onto string states in Ref. [4]:

$$\begin{aligned} B(\mathbf{0},t) &\to \pm i\tilde{\Lambda}^2\partial_0\varphi(0,t),\\ B^*(\mathbf{0},t) &\to \mp i\tilde{\Lambda}^2\partial_0\varphi^*(0,t),\\ B^3(\mathbf{0},t) &\to \pm\tilde{\Lambda}'^2 i\partial_0\varphi(0,t)\partial_z\varphi^*(0,t) + \text{H.c.}, \end{aligned} \tag{A4}$$

$t=\pm\frac{T}{2}$. Note that neither $V^{sa}_{1^+11}(r)$ nor $V^{sb}_{1^+11}(r)$ depend on the values of $\tilde{\Lambda}^2$ or $\tilde{\Lambda}'^2$. $V^{sa}_{1^+11}(r)$ is not sensitive to the sign ambiguity of the mapping either; however, $V^{sb}_{1^+10}(r)$ is, which produces a sign ambiguity in it. Recall that $V_{\Pi_u} - V_{\Sigma_u^-} = -\frac{2\pi}{r}$ in EST. Once these substitutions are carried out in Eq. (A1), and the QCD vacuum averages $\langle\cdots\rangle_\square$ replaced by the string vacuum average $\langle\cdots\rangle$, a simple (tree-level) calculation in EST leads to Eq. (14) [34].

[1] R. L. Jaffe and K. Johnson, Phys. Lett. **60B**, 201 (1976).
[2] E. Braaten, C. Langmack, and D. H. Smith, Phys. Rev. D **90**, 014044 (2014).
[3] M. Berwein, N. Brambilla, J. Tarrús Castellà, and A. Vairo, Phys. Rev. D **92**, 114019 (2015).
[4] R. Oncala and J. Soto, Phys. Rev. D **96**, 014004 (2017).
[5] J. Soto, Nucl. Part. Phys. Proc. **294–296**, 87 (2018).
[6] N. Brambilla, W. K. Lai, J. Segovia, J. Tarrús Castellà, and A. Vairo, Phys. Rev. D **99**, 014017 (2019); **101**, 099902(E) (2020).
[7] J. Soto and J. Tarrús Castellà, Phys. Rev. D **102**, 014012 (2020).
[8] K. J. Juge, J. Kuti, and C. J. Morningstar, Phys. Rev. Lett. **82**, 4400 (1999).
[9] E. Braaten, C. Langmack, and D. H. Smith, Phys. Rev. Lett. **112**, 222001 (2014).
[10] J. Tarrús Castellà and E. Passemar, Phys. Rev. D **104**, 034019 (2021).
[11] N. Brambilla, W. K. Lai, A. Mohapatra, and A. Vairo, Phys. Rev. D **107**, 054034 (2023).
[12] A. Pineda and J. Tarrús Castellà, Phys. Rev. D **100**, 054021 (2019).
[13] N. Brambilla, S. Eidelman, C. Hanhart, A. Nefediev, C. P. Shen, C. E. Thomas, A. Vairo, and C. Z. Yuan, Phys. Rep. **873**, 1 (2020).
[14] H. X. Chen, W. Chen, X. Liu, Y. R. Liu, and S. L. Zhu, Rept. Prog. Phys. **86**, 026201 (2023).
[15] N. Brambilla, W. K. Lai, J. Segovia, and J. Tarrús Castellà, Phys. Rev. D **101**, 054040 (2020).
[16] M. Luscher and P. Weisz, J. High Energy Phys. 07 (2002) 049.
[17] M. Luscher and P. Weisz, J. High Energy Phys. 07 (2004) 014.
[18] G. Perez-Nadal and J. Soto, Phys. Rev. D **79**, 114002 (2009).
[19] N. Brambilla, M. Groher, H. E. Martinez, and A. Vairo, Phys. Rev. D **90**, 114032 (2014).
[20] G. K. C. Cheung, C. O'Hara, G. Moir, M. Peardon, S. M. Ryan, C. E. Thomas, and D. Tims (Hadron Spectrum Collaboration), J. High Energy Phys. 12 (2016) 089.
[21] J. Tarrús Castellà, AIP Conf. Proc. **2249**, 020008 (2020).
[22] P. Solé Campreciós, Heavy hybrids mesons in NRQCD: Fine and hyperfine structure, Bachelor thesis, Universitat de Barcelona, 2017.
[23] P. Molina Grífols, Spin-dependent effects on the hyperfine structure in heavy hybrid mesons, Bachelor thesis, Universitat de Barcelona, 2021.
[24] A. Pineda and J. Soto, Nucl. Phys. B, Proc. Suppl. **64**, 428 (1998).
[25] N. Brambilla, A. Pineda, J. Soto, and A. Vairo, Nucl. Phys. **B566**, 275 (2000).
[26] K. J. Juge, J. Kuti, and C. Morningstar, Phys. Rev. Lett. **90**, 161601 (2003).
[27] G. S. Bali and A. Pineda, Phys. Rev. D **69**, 094001 (2004).
[28] S. Capitani, O. Philipsen, C. Reisinger, C. Riehl, and M. Wagner, Phys. Rev. D **99**, 034502 (2019).
[29] C. Schlosser and M. Wagner, Phys. Rev. D **105**, 054503 (2022).
[30] M. Luscher, K. Symanzik, and P. Weisz, Nucl. Phys. **B173**, 365 (1980).
[31] A. V. Manohar, Phys. Rev. D **56**, 230 (1997).
[32] G. Amoros, M. Beneke, and M. Neubert, Phys. Lett. B **401**, 81 (1997).
[33] A. G. Grozin, P. Marquard, J. H. Piclum, and M. Steinhauser, Nucl. Phys. **B789**, 277 (2008).
[34] J. Castillo Uviña, Spin dependent potential of the heavy hybird mesons, Bachelor thesis, Universitat de Barcelona, 2020.
[35] Y. Koma and M. Koma, Proc. Sci. LAT2009 (**2009**) 122.
[36] Y. Koma and M. Koma, Nucl. Phys. **B769**, 79 (2007).

[37] S. Tomàs Valls, Spectrum of heavy quarkonium hybrids: Hyperfine splitting, Bachelor thesis, Universitat de Barcelona, 2021.

[38] S. M. Ryan and D. J. Wilson (Hadron Spectrum Collaboration), J. High Energy Phys. 02 (2021) 214.

[39] L. Liu, G. Moir, M. Peardon, S. M. Ryan, C. E. Thomas, P. Vilaseca, J. J. Dudek, R. G. Edwards, B. Joó, and D. G. Richards (Hadron Spectrum Collaboration), J. High Energy Phys. 07 (2012) 126.

[40] L. Müller, O. Philipsen, C. Reisinger, and M. Wagner, Phys. Rev. D **100**, 054503 (2019).

[41] G. S. Bali, B. Bolder, N. Eicker, T. Lippert, B. Orth, P. Ueberholz, K. Schilling, and T. Struckmann (TXL and T(X)L Collaborations), Phys. Rev. D **62**, 054503 (2000).

[42] M. Dalla Brida, R. Höllwieser, F. Knechtli, T. Korzec, A. Nada, A. Ramos, S. Sint, and R. Sommer (ALPHA Collaboration), Eur. Phys. J. C **82**, 1092 (2022).

[43] G. Ray and C. McNeile, Proc. Sci. LATTICE2021 (**2022**) 240.

[44] C. A. Meyer and E. S. Swanson, Prog. Part. Nucl. Phys. **82**, 21 (2015).